Corrosion Science 158 (2019) 108108

Contents lists available at ScienceDirect

Corrosion Science

journal homepage: www.elsevier.com/locate/corsci

A comprehensive study of the spatial distribution of the galvanic protection current supplied by zinc layer anodes applied to steel-reinforced concrete structures

D. Garcia[a], S. Laurens[a,*], S. Panin[b]

[a] Université de Toulouse, UPS, INSA, LMDC 135 avenue de Rangueil, 31077, Toulouse Cedex 4, France
[b] R3S, N°18 ZA Les Pignès, 09270, Mazères, France

ARTICLE INFO

Keywords:
Steel reinforced concrete
Cathodic protection
Modelling
Oxygen supply
Numerical simulation

ABSTRACT

Improving the design of cathodic protection systems applied to steel-reinforced concrete structures requires a comprehensive description of the on-going physical phenomena in order to achieve robust engineering models. In this context, this paper deals with one highly relevant question of cathodic protection design: the spatial distribution of the protecting current over the reinforcing steel. The issue is addressed here, for the specific case of zinc layer anodes, by means of experimental tests performed on simple laboratory specimens, together with numerical simulations resulting from theoretical analysis of the physical problem. Particular attention is given to oxygen availability and concrete moisture.

1. Introduction

It is well known that steel corrosion leads to accelerated deterioration of reinforced concrete structures. Due to the high alkalinity of the concrete pore solution, a thin, compact and stable passive oxide layer is formed on the steel surface. This phenomenon is referred to as steel passivation, which actually corresponds to a uniform corrosion state, but with negligible corrosion rates. The local dissolution of the passive film induced by partial carbonation of the concrete cover or local high chloride concentration generates the condition of macrocell (or localized) corrosion. In other words, when an active (depassivated) steel area is formed, its corrosion rate is significantly increased by galvanic exchanges with the surrounding passive steel. In addition to structural problems resulting from steel section losses, corrosion-induced rust expansion may cause other severe damage to RC structures, such as concrete cover cracking, spalling and delamination [1].

In this context, the implementation of cathodic protection (CP) in RC structures has grown substantially during the past two decades. Several design standards have been proposed for cathodic protection, such as the NACE SP0216 and SP0290 [2] or the EN 12,696 standard [3]. Generally speaking, CP design and performance criteria, as well as monitoring methods, are based on empirical assumptions that do not allow for optimization of the protection system. Therefore, improving the design and control of CP systems requires a comprehensive description of on-going physical phenomena from the scientific community in order to achieve robust engineering models [4,5].

The corrosion of steel in concrete is an electrochemical process in which the dissolution of steel constitutes the anodic reaction (Eq. (1)), which provides electrons that are consumed by the cathodic reaction corresponding to the reduction of oxygen dissolved in the interstitial solution of the concrete (Eq. (2)).

$$Fe \rightarrow Fe^{2+} + 2e^{-} \quad (1)$$

$$O_2 + 2H_2O + 4e^{-} \rightarrow 4OH^{-} \quad (2)$$

Two main types of steel corrosion are usually associated with reinforced concrete structures:

- Microcell corrosion: anodic and cathodic areas are immediately adjacent along the reinforcing bar; each electron produced by steel dissolution is consumed locally by oxygen reduction involving a negligible ohmic drop between anodic and cathodic areas. Both anodic and cathodic areas reach the same electrochemical potential (E_{corr}), the global potential field is uniform in the concrete volume and, consequently, no ionic current is produced.
- Macrocell (or galvanic) corrosion: anodic and cathodic areas at the steel-concrete interface are spatially separated, so there is an electrolytic resistance between them. Therefore, anodic and cathodic half-cells do not reach the same potential, resulting in a potential gradient and a galvanic corrosion current in the concrete volume.

* Corresponding author.
E-mail address: stephane.laurens@insa-toulouse.fr (S. Laurens).

https://doi.org/10.1016/j.corsci.2019.108108
Received 6 May 2019; Received in revised form 11 July 2019; Accepted 19 July 2019
Available online 20 July 2019
0010-938X/

Actually, only uniform passive steel can be regarded as a uniform corrosion system in reinforced concrete structures. Any other corrosion system, involving both active and passive steel areas, has to be considered as a macrocell (or galvanic) system. It must be added that, whatever the environmental exposure, steel bars in concrete cannot be uniformly depassivated, which means that a uniform active state is not likely to occur. Obviously, a long-term galvanic process could lead to generalized corrosion by growth and coalescence of active areas, but such a case is associated with very advanced deterioration of the structure.

The theoretical concepts exposed above for steel corrosion can be extended to galvanic protection. A galvanic protection is actually a macrocell corrosion system in which the natural oxidation of zinc, connected to the reinforcing steel network, provides electrons consumed by oxygen reduction primarily at the passive steel-concrete interface. Connecting zinc anodes to reinforcing bars in concrete results in their mutual polarization. Since zinc in concrete is characterized by a modest electrochemical potential of about $-1000\,mV\ vs\ SCE$ [6], passive and active steel areas are subjected to cathodic polarization and zinc anodes undergo anodic polarization. Therefore, the macrocell corrosion current between active and passive steel areas is mitigated, or may even be annihilated if the galvanic protection system is correctly designed.

Physically, galvanic protection applied to corroding steel in concrete can be seen as a three-component system: galvanic anode + active steel + passive steel. Compared to the pre-existing macrocell system formed by active and passive steel areas, an additional macrocell current flows from the sacrificial anode towards the reinforcing steel bars when they are connected. The potential gradient in the concrete volume is also modified by the connection of this third component and the whole system reaches a new electrochemical equilibrium.

The equilibrium achieved is defined by the rates of electrochemical reactions at the different interfaces, the associated ionic current, and the potential field in the concrete volume. The equilibrium is controlled by three predominant influencing factors:

- the respective electrochemical behaviours of the three components; this is referred to as charge transfer control;
- the field of electrical resistivity in the concrete volume;
- the oxygen supply by diffusion through the partially-saturated concrete matrix towards the cathodic regions at the steel-concrete interface; this is referred to as mass transfer control.

According to Raupach [7], the degree of pore water saturation in the cementitious matrix and its influence on oxygen diffusion properties are key parameters for modelling the electrochemical process occurring in reinforcement corrosion. Moreover, the saturation degree of concrete is the main influencing factor of electrical resistivity. Both steel corrosion and cathodic protection in reinforced concrete are highly dependent on oxygen diffusion and concrete resistivity but there is some competition between these influencing factors. A dry concrete facilitates the oxygen supply (by oxygen diffusion in the gaseous phase) but it is also associated with high electrical resistivity due to a continuity breakdown in the liquid phase of the cementitious pore network and limiting galvanic exchanges. Therefore, in dry concrete, corrosion and cathodic protection are controlled by electrical and electrochemical phenomena, since oxygen supply is not a limiting factor. Conversely, in a water-saturated concrete, the transport of dissolved oxygen in water filled pores is very slow, while the electrolytic conductivity is very high [8]. In this case, galvanic exchanges are not controlled by electrical resistivity but by the rate of the cathodic reaction, which is limited by the rate of oxygen diffusion towards the steel reinforcements.

In the literature, the saturation value of cathodic current is introduced as the limiting current of oxygen reduction (i_{lim}). This current may be simply deduced from Fick's first law (mass transport) and Faraday's constant (electrochemistry) as follows:

$$J_{O_2} = -D_e \nabla c \tag{3}$$

$$i_{lim} = -4F\, J_{O_2} \tag{4}$$

where:

- J_{O_2} is the oxygen flux flowing through steel-concrete interface ($mol.\ m^{-2}.\ s^{-1}$),
- c is the local oxygen concentration ($mol.\ m^{-3}$),
- D_e is the effective diffusion coefficient of oxygen ($m^2.\ s^{-1}$),
- F is the Faraday constant ($= 96485\,C.\ mol^{-1}$).

Several authors consider the oxygen diffusion as a one-dimensional problem with total consumption of oxygen at the steel-concrete interface to simplify the estimation of concentration gradient in the limiting current expression. However, these assumptions are only justified in fully saturated concrete involving a linear concentration distribution through concrete cover. In partly saturated concrete, the limiting current of oxygen reduction may be evaluated locally by using appropriate 3D numerical methods to assess the concentration distribution in the concrete volume. Therefore, the global electrochemical equilibrium relative to a galvanic protection system is a three-dimensional non-linear physical problem. Computing such a 3D equilibrium requires the development of appropriate numerical models [9,10].

Electrochemical modelling and numerical simulation of cathodic protection implemented in RC structures is a relatively recent research field. A few research works can be found on the numerical simulation of coupled effects of the electrochemical process and oxygen diffusion through partly saturated concrete to describe a corroding system [11]. However, the literature is very scarce regarding the response of macrocell corrosion systems under cathodic polarization. This topic is nevertheless of major importance regarding the aim of optimizing the design of cathodic protection in RC structures.

In a robust computational model of steel corrosion in concrete and/or a related cathodic protection system, the three main influencing phenomena described above have to be taken into consideration to provide realistic numerical simulations and to assess the cathodic polarization level of the reinforcing network [8]:

- Electrochemical processes at the different metal-concrete interfaces: active steel/concrete, passive steel/concrete, CP anodic system/concrete (such as zinc/concrete);
- Oxygen diffusion correlated to capillary water transport in the cementitious matrix;
- The field of electrical resistivity, which is also directly influenced by water transport.

In the work presented here, the specific case of galvanic protection by means of zinc layer anodes (ZLA) was studied giving special attention to the impact of oxygen supply on the global macrocell equilibrium. The spatial distribution of the protecting current from the galvanic anode towards the steel reinforcement and the potential field was studied in relation with oxygen availability in the concrete volume. Section 2 of this paper presents original experiments carried out to demonstrate the relevance of oxygen availability as a predominant influencing factor of galvanic cathodic protection. In section 3, the theoretical background necessary to achieve effective numerical simulations is reported. Section 4 demonstrates the robustness of the numerical simulations by comparing them with the experiments described in section 2.

2. Experimental investigations on concrete specimens

2.1. Experimental protocol

The following section presents some experiments specifically designed to highlight the relevance of taking the oxygen supply into account as a predominant control parameter in the design of galvanic protection systems. Experiments were carried out on a small concrete

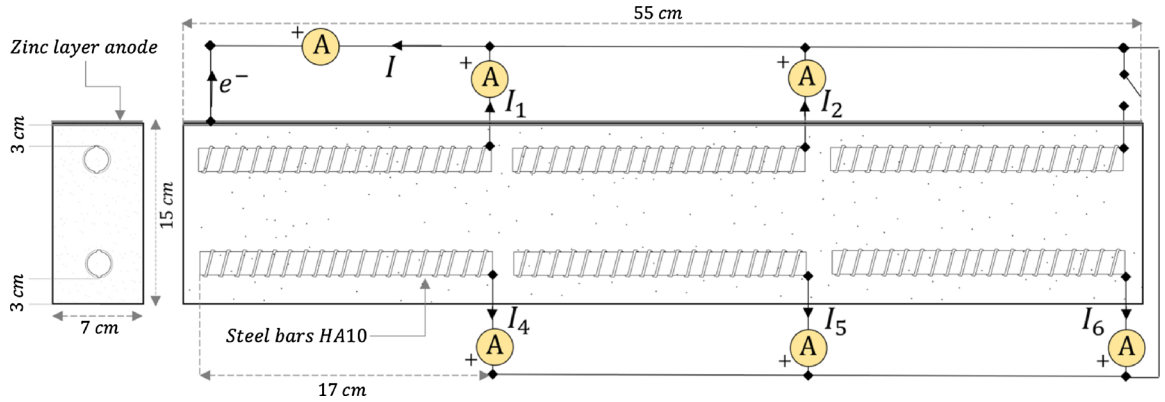

Fig. 1. Experimental specimen: small concrete beam in dry condition (easy oxygen transport) embedding 6 independent passive steel rods (test1).

beam (Fig. 1) in which six bars were embedded in two layers: 3 upper steel bars (labelled 1 to 3) and three lower steel bars (labelled 4 to 6). The dimensions of the concrete slab were $55 \times 7 \times 15\,cm^3$. All steel bars were 1 cm in diameter and 17 cm high. The concrete cover above the upper steel layer was 3 cm, while the lower steel layer depth was 11 cm from the top side of the bars to the top concrete surface. The concrete mix proportions were as follows: a water-cement ratio of 0.6, an aggregate-cement ratio of 2.8 and a sand-cement ratio of 2.0. Curing consisted of covering the specimen with plastic sheathing for 7 days. A zinc sheet backed with an ion conductive adhesive paste (ZLA) was applied to the top surface of the specimen.

All the bars were independent, but welded metallic wires allowed for any electrical connection between two or more steel bars, making it possible to generate different macrocell systems. In the following experiments, all the steel bars were connected, except for bar 3, as shown in Fig. 1. Bar 3 of the upper layer was voluntarily unconnected in order to cause some non-uniformity of the polarization field due to the asymmetric reinforcing network. In particular, the unconnected bar 3 did not produce any masking effect on the protection current in this configuration.

The bar output currents (I_1, I_2, I_4, I_5, I_6) were collected separately using a BioLogic® VMP3 multi-channel potentiostat-galvanostat. The ZRA technique was used to record the current flowing between the working electrode (zinc layer anode) and each steel bar. This protocol enabled the spatial distribution of the protection current supplied by the ZLA sheet over the 5 connected steel rods to be reliably assessed.

Numerous tests were conducted on this specimen to compare numerical and experimental results and to confirm experimental observations on various systems. However, only two of the most typical results summarizing experimental observations are presented below. For the whole duration of the tests, the reinforcing network was kept in a passive electrochemical state.

These experiments collected the protection current received by each of the five passive steel bars embedded in a concrete slab under two different environmental conditions:

- **Test 1**: a concrete beam at hydric equilibrium in an air-conditioned room (Fig. 1), involving a fairly uniform moisture saturation degree of about 60% (measured on small concrete test cylinders coming from the same concrete mix). In such environmental conditions, oxygen could be easily transported by diffusion towards all the steel rods in the concrete beam.
- **Test 2**: a partially coated concrete beam with fully moisture saturated concrete around the upper steel bars (Fig. 2). The concrete beam was first immersed in tap water until its mass stabilized. Then, an epoxy resin was applied to the upper part of the beam surface in order to prevent oxygen diffusion to the upper steel layer. Gas transport through the cementitious matrix was only allowed through the lower part of the beam, meaning that the lower steel layer received much more oxygen than the upper layer. The water saturation field in the concrete volume is not directly measurable but, since the resin coating also avoided any drying process in the upper part of the beam, it can reasonably be considered that concrete was fully saturated around the upper steel bars, while it was only partially saturated around the lower steel layer.

2.2. Experimental results

The output currents from each connected bar were monitored for 70 h for both experiments. The results for Test 1 (unlimited oxygen supply) and Test 2 (limited oxygen supply at the upper steel layer) are presented in Figs. 3 and 4, respectively. The averaged stabilized current distribution for both experiments is summarized in Fig. 5 as fractions (in %) of the global protection current supplied by the ZLA.

The global macrocell current flowing from the zinc layer anode to the reinforcing bars for unlimited oxygen supply (Test 1) was 1.79 mA, corresponding to a mean anodic current density of 47 $mA.\,m^{-2}$ of zinc. According to Faraday's law, the rate of zinc dissolution in this specific galvanic protection system was estimated at $500\,g.m^{-2}.year^{-1}$.

Regarding the results of Test 1 (unlimited oxygen supply in the concrete beam), the total cathodic current collected for the upper steel bars ($-1.18\,mA$, corresponding to an averaged value of $-110\,mA.\,m^{-2}$ of steel) was almost two times that received by the lower steel bars ($-0.61\,mA$, corresponding to an averaged value of $-39\,mA.\,m^{-2}$ of steel) since the upper layer was closer to the sacrificial anode. In this test, the ohmic resistance due to the electrical resistivity of the concrete was therefore the predominant control parameter of the galvanic system. Regarding the lower layer (far from the ZLA), it can be observed that the protection current collected by passive bar 6 was 30% higher than the currents distributed over bars 4 and 5. This resulted from the connection asymmetry. As bar 3 was unconnected, it did not receive any protection current and therefore did not induce any masking effect. Another effect of the disconnection of bar 3 was observed on the upper layer steel bars, where bar 2 received a significantly higher current than bar 1.

Nevertheless, the first important observation of this research work is that, in the conditions of Test 1, the lower steel bars collected a significant amount of the total protection current provided by the sacrificial anode: about 65% of the protection current was spread over the closest bars (upper), against 35% over the lower layer. Obviously, these ratios would be slightly different if bar 3 was connected in the electrochemical circuit, but it would not make the current received by the lower steel bars negligible.

In the condition of limited oxygen supply at the upper steel layer (Test 2), the distribution of the galvanic protection current was completely modified with respect to that relative to Test 1. The ZLA provided a total protection current of 2.55 mA. In Fig. 4, it can be clearly observed that, despite their immediate vicinity to the sacrificial anode,

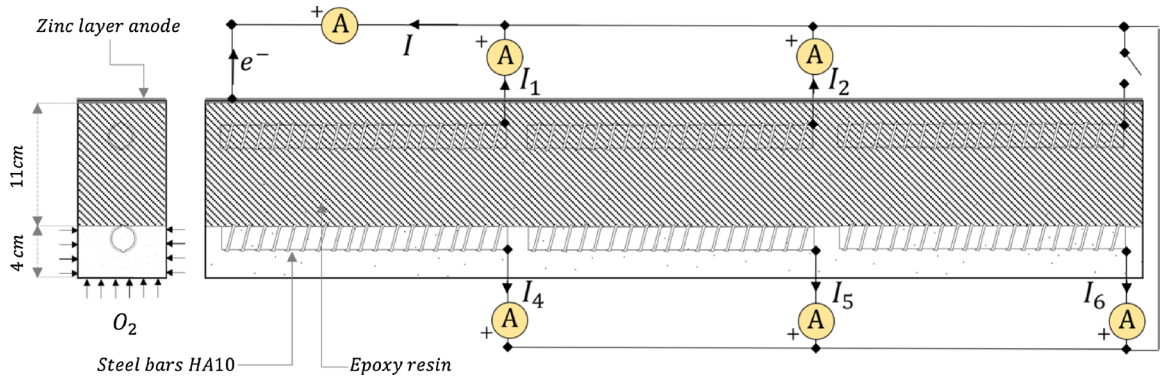

Fig. 2. Partially coated concrete beam with very low rate of oxygen transport towards the upper steel layout (test 2).

bars 1 and 2 received very little galvanic protection current (total value of $-0.15\,mA$) while the lower layer collects a high value of protection current ($-2.40\,mA$).

Fig. 5 provides a quick comparison of the different current distributions observed for Test 1 and Test 2. The upper steel bars collected about 65% of the galvanic current supplied by the ZLA in the conditions of Test 1. Conversely, the lower steel bars collected about 95% of the protection current in the condition of Test 2.

The protection current density collected by the upper steel bars dropped from $-110\,\mathrm{mA.m^{-2}}$ of steel, in the case of unlimited oxygen access, to $-13\,\mathrm{mA.\ m^{-2}}$ when oxygen access was limited by water saturation and epoxy coating. Conversely, the protection current received by the lower steel layer became substantially higher, reaching $-150\,\mathrm{mA.m^{-2}}$ of steel while the upper steel bars were no longer able to consume electrons by oxygen reduction. In that case, a redistribution of the protection current was observed towards steel areas where oxygen concentration was sufficient to fuel the cathodic reaction.

It has to be noted here that the global galvanic protection currents flowing from the zinc layer anode to the reinforcing bars cannot be directly compared for Test 1 and Test 2 ($-1.8\,mA$ and $-2.55\,mA$, respectively) since the moisture contents of the concrete were different. The anodic current produced by the zinc anode is likely to be higher in a fully saturated concrete with low electrical resistivity but, at the same time, the electrical path to reach areas with high oxygen concentration was longer. In these experiments, the lower global resistivity in the case of Test 2 results in a higher galvanic protection current. Nevertheless, generally speaking, the global galvanic protection current and its distribution over the steel reinforcements result from some balance between:

- The electrochemical behaviours proper to the different system components;
- Resistivity effects
- The spatial locations of the cathodic reactions (high oxygen concentration).

In such conditions, a relevant assessment of the galvanic protection current supplied by the sacrificial anode requires appropriate numerical simulations based on the coupling between electrical and electrochemical phenomena, and the oxygen diffusion through partly saturated concrete.

3. Numerical simulation approaches

This section deals with the elementary physical concepts needed to perform relevant numerical simulations of the preceding experiments. Three different modelling approaches are proposed based on several assumptions:

- A first modelling approach, labelled ***Electrochemical model***, assumes an unlimited oxygen supply at each steel-concrete interface. In such a model, the system equilibrium is controlled only by resistivity effects and electrochemical behaviours (charge transfer) of the different metal-concrete interfaces.

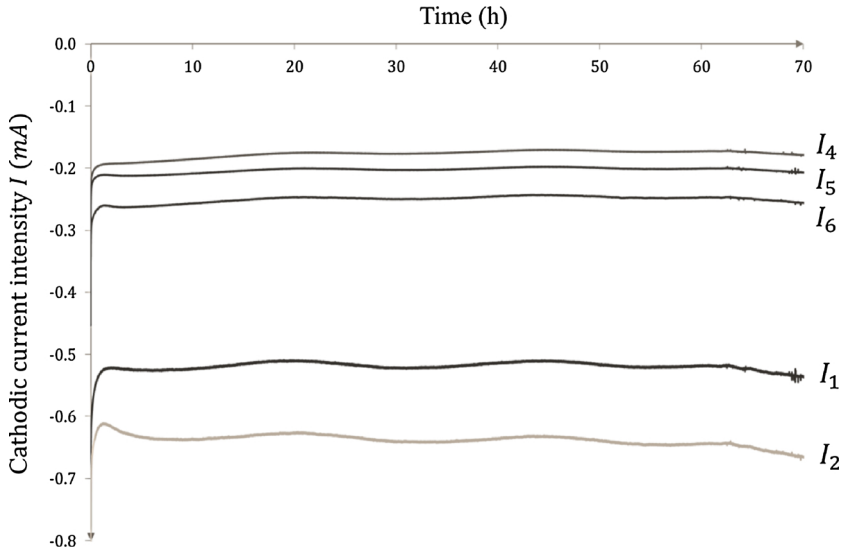

Fig. 3. Monitoring of the protection current collected by each steel bar - Test 1 (Unlimited oxygen supply).

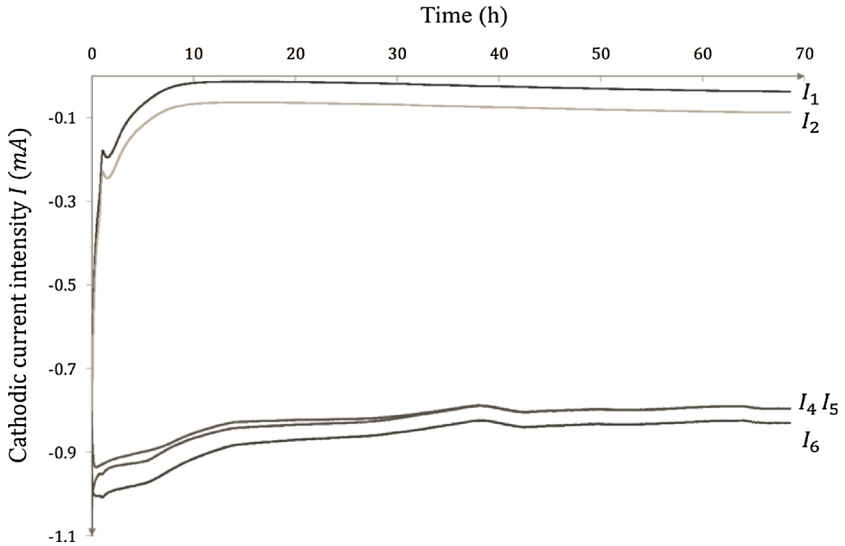

Fig. 4. Monitoring of the protection current collected by each steel bar - Test 2 (Limited oxygen supply at the upper steel layer).

- A second approach, labelled ***Diffusion model***, assumes that all the oxygen reaching steel bars is consumed; here, the system equilibrium is cathodically controlled by the diffusion kinetics of oxygen through concrete, i.e. by the limiting current of oxygen reduction.
- A coupled modelling approach, labelled ***Multiphysics model***, addressing the interaction between electrical, electrochemical and oxygen diffusion phenomena.

The first two approaches (Electrochemical and Diffusion models) are simplified models, but may be regarded as reliable to estimate the galvanic current in some environmental conditions. Simulations based on the Electrochemical model are relevant in cases of fairly dry concrete, where oxygen availability is not a limiting factor. Conversely, for very wet or saturated concretes, the Diffusion model may be sufficient since the galvanic equilibrium is totally controlled by the oxygen transport (cathodic control). Therefore, these simplified modelling approaches should not be systematically proscribed since they require significantly shorter computation time. However, for saturation degrees between approximately 60% and 90%, electrochemical effects and oxygen diffusion are in competition for equilibrium control and the coupled modelling approach is necessary to achieve relevant simulations.

In the following, numerical simulations were carried out by using the commercially-available Finite Elements software Comsol Mutiphysics®. All the calculations were performed in steady state conditions using the *Electric current* toolbox (EC) for electrochemical phenomena and the *Transport of diluted species in porous media* toolbox (TDS.p) for oxygen diffusion.

3.1. Electrochemical model

At an electrochemical interface, if the charge transfer is rate limiting (no mass transport limitation), the steel surface concentrations are equal to the bulk concentration. The polarization behaviour of such uniform systems may be modelled by the usual Butler-Volmer equation as follows (Eq. (5)) [12]:

$$i = i_{corr}\left(\exp\left(\frac{\mathrm{Log}(10)(E - E_{corr})}{\beta_a}\right) - \exp\left(-\frac{\mathrm{Log}(10)(E - E_{corr})}{\beta_c}\right)\right) \quad (5)$$

where:

- $i\ (A.\ m^{-2})$ is the net current density flowing through the metal-electrolyte interface of the uniform corrosion system polarized at

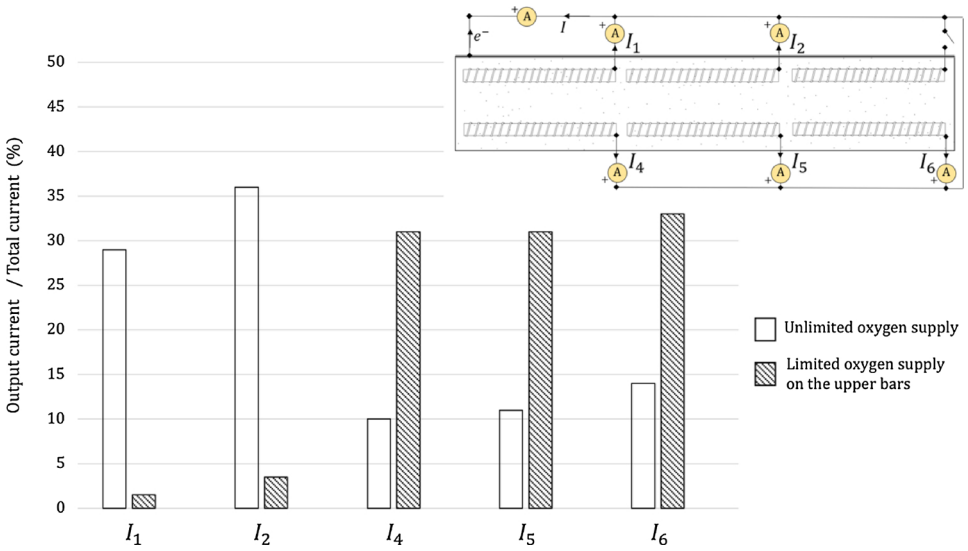

Fig. 5. Output currents distributions for oxygen unlimited (Test 1) and oxygen limited (Test 2) oxygen supply.

potential $E\ (V)$,

- $i_{corr}\ (A.\ m^{-2})$ is the corrosion current density at the corrosion potential $E_{corr}\ (V)$,

- β_a and $\beta_c\ (V.\ dec^{-1})$ are the anodic and cathodic Tafel slopes of the electrochemical system, respectively.

The Butler-Volmer equation actually corresponds to the algebraic sum of the current densities associated with the anodic reaction of metal dissolution and the cathodic reaction of oxygen reduction.

The steel bars are considered as perfect electrical conductors and, thus, only the steel-concrete interface is modelled. Passive steel boundaries are modelled by the Butler-Volmer equation using an appropriate set of parameters. The electrochemical parameters involved in this work reflect the global orders of magnitude found from literature data [13]. Only the quantitative aspect of numerical results may be changed by the variability of these parameters.

Regarding the polarization behaviour of zinc anodes in galvanic protection, the zinc–concrete interface is almost always assumed to be non-polarizable and the zinc anode is fixed at a constant potential in numerical simulations. However, the specific electrochemical properties of ZLA have recently been measured [6], making it possible to also model the sacrificial anode as a Butler-Volmer boundary. Table 1 summarizes the electrochemical parameters involved in the following simulations and Fig. 6 plots the relative polarization curves.

In the concrete volume, the local Ohm's law (Eq. (6)) and charge conservation (Eq. (7)) govern electrical phenomena:

$$i = -\frac{1}{\rho}\nabla E \tag{6}$$

$$\nabla .\ i = 0 \tag{7}$$

where i is the local current density vector $(A.m^{-2})$, E is the electric potential field (V) and ρ is the electrical resistivity of concrete $(\Omega .\ m)$.

In order to simplify the study, the concrete is assumed to be a homogeneous, isotropic, conductive material and so the electrical resistivity of concrete is considered as uniformly distributed. Therefore, from Eqs. (6) and (7), the potential distribution inside the concrete volume can be described by Laplace's Equation (Eq. (8)):

$$\nabla^2 E = 0 \tag{8}$$

The electrical resistivity of the concrete is a predominant parameter of the galvanic system equilibrium since it strongly influences the ionic macrocell current intensity flowing from the galvanic anodes and consequently the zinc dissolution kinetics. Concrete resistivity depends strongly on the volume water content, w, according to a power law. Based on experimental results of the French research project *SENSO* on a large range of concrete mixtures [14], the empirical relationship between water content and electrical resistivity of concrete involved in this work is as follows (Eq. (9)) :

$$\rho = 0.437\, w^{-2.53} \tag{9}$$

and:

$$w = p.\ S_r \tag{10}$$

where S_r is the water saturation degree, p the porosity of the concrete and w its moisture content, all these quantities being dimensionless.

The porosity of the concrete beam presented in section 2 was 18%.

Table 1
Butler–Volmer parameters used in numerical simulations.

BV parameters	Passive steel	Zinc sheet
$E_{corr}\ (V)$	− 0.1	− 1.01
$i_{corr}\ (A.\ m^{-2})$	10^{-4}	$4.0\,10^{-3}$
$\beta_a\ (V.\ dec^{-1})$	1	0.019
$\beta_c\ (V.\ dec^{-1})$	0.2	0.05

Therefore, from Eqs. (9) and (10), it is possible to assess the relationship between electrical resistivity and saturation degree (Fig. 7) to be implemented in the following numerical simulations.

The current intensity $I_i\ (A)$ collected by a specific steel rod i, may be calculated by surface integration of the normal cathodic current density at the steel rod-concrete interface $i_{n,i}\ (A.\ m^{-2})$ as follows (Eq. (11)):

$$I_i = \iint_{S_i} i_{n,i}\, dS \tag{11}$$

The global protection current I_p is then achieved by adding the locally-collected currents I_i (Eq. (12)):

$$I_p = \sum_i I_i \tag{12}$$

The global current can also be calculated by surface integration of the normal anodic current density (I_z) produced at the zinc-concrete interface · Due to electro-neutrality, the anodic current I_z has to be balanced by the cathodic current I_p as follows (Eq. (13)):

$$I_z = -I_p \tag{13}$$

Therefore, the relative error between I_z and I_p is a measure of the convergence quality in the numerical simulation.

The dimensions of numerical specimen were identical to those of the experimental concrete beams described in section 2. The model geometry and the different boundary conditions involved in the numerical simulation performed according to the Electrochemical model are illustrated in Fig. 8.

3.2. Diffusion model: limiting current of oxygen reduction I_{lim,O_2}

The diffusion model approach is based on the assumption that all the oxygen reaching any steel rod is consumed instantaneously, i.e. the oxygen concentration, c, at any steel-concrete interface is always zero. Therefore, the global cathodic current produced on the all the passive steel is limited by the oxygen diffusion kinetics in the concrete volume. Consequently, the protection current supplied by the ZLA is also controlled by oxygen diffusion since electro-neutrality has to be preserved. In this condition, the calculation of the cathodic current produced by each steel rod, which is implicitly equal to the galvanic protection current collected, may simply be deduced from the maximum oxygen flux at the steel-concrete interface. The global protection current achieved is then the global limiting current of oxygen reduction I_{lim,O_2}, which can be assessed by adding the local diffusion flows.

The theoretical details presented below are inspired by Aachib et al. [15], who developed a numerical approach to evaluate the oxygen flux through partly saturated media, based on experimental investigations [16].

Oxygen transport through the concrete cover is considered as a pure diffusion problem here, the convective part being neglected because of the assumption that water saturation of concrete is uniform and invariant. Therefore, transport of pore solution was not modelled in this study. Fick's first law, adapted to porous media, and the principle of mass conservation govern diffusion phenomena in the concrete volume, leading to the following general equation (Eq. (14)):

$$p_{eff}\frac{\partial c}{\partial t} = D_e\, \nabla^2 c \tag{14}$$

where:

- c is the local oxygen concentration $(mol.\ m^{-3})$,
- p_{eff} is the effective diffusion porosity,
- D_e is the effective diffusion coefficient $(m^2.\ s^{-1})$.

The effective diffusion porosity is used here to take account of both the oxygen flux in gaseous phase and the flux of oxygen dissolved in water-filled pore space (Eq. (15))

$$p_{eff} = p_a + K_H.\ p_w \tag{15}$$

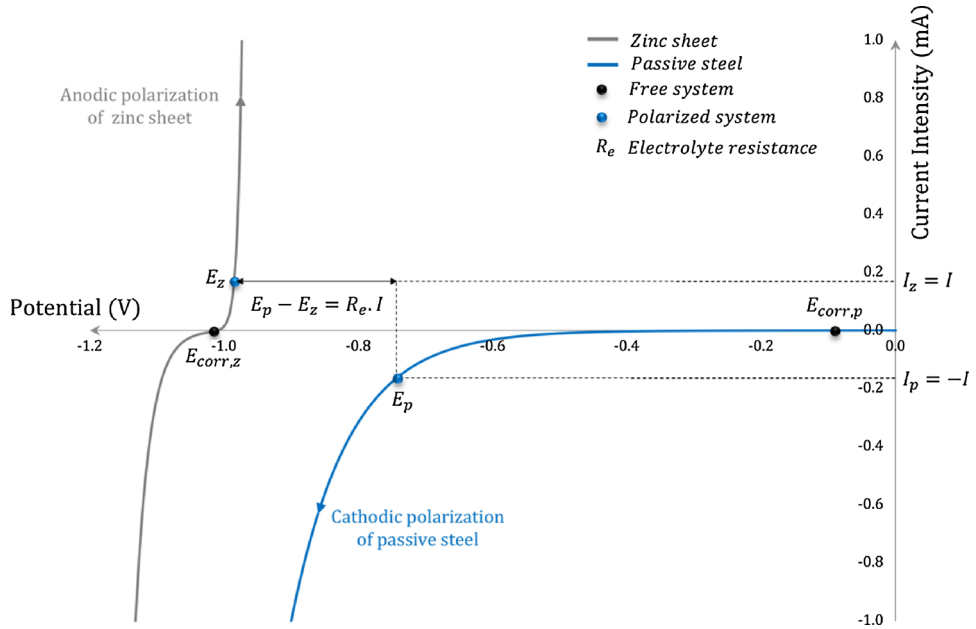

Fig. 6. Qualitative electrochemical behaviours of ZLA and passive steel.

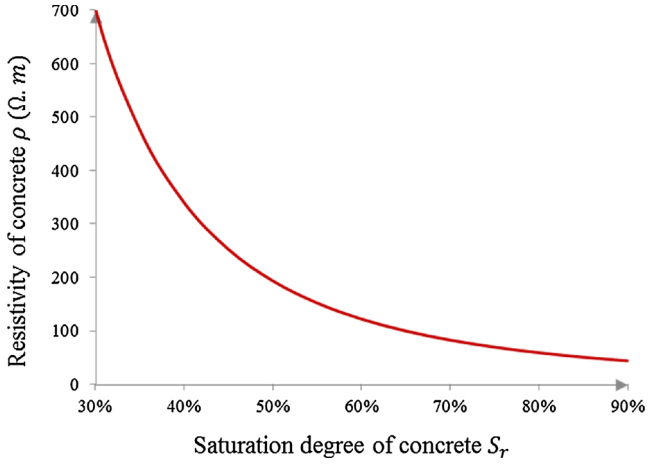

Fig. 7. Empirical relationship between electrical resistivity and saturation degree of concrete.

with

$$p_a = p.(1 - S_r) \tag{16}$$

$$p_w = p.S_r \tag{17}$$

where p_a and p_w are the volumetric air and water contents respectively, S_r is the degree of saturation, p is the concrete porosity and K_H is the dimensionless form of Henry's equilibrium constant. The latter parameter depends on temperature T ($°C$) and atmospheric pressure p_{atm} (Pa) and may be defined by the ratio of the oxygen concentration dissolved in water c_{aq} ($mol.\ m^{-3}$) to the oxygen concentration in air c_g ($mol.\ m^{-3}$) as follows (Eq. (17)):

$$K_H = \frac{c_{aq}}{c_g} \tag{17}$$

At $T = 20\,°C$, the oxygen concentration in air is (Eq. (18)):

$$c_g = 21\%.\frac{p_{atm}}{R(T + 273)} = 8.73\,mol.\ m^{-3} \tag{18}$$

where R is the universal gas constant ($=8.314\,J.\ mol^{-1}.\ K^{-1}$) and p_{atm} is

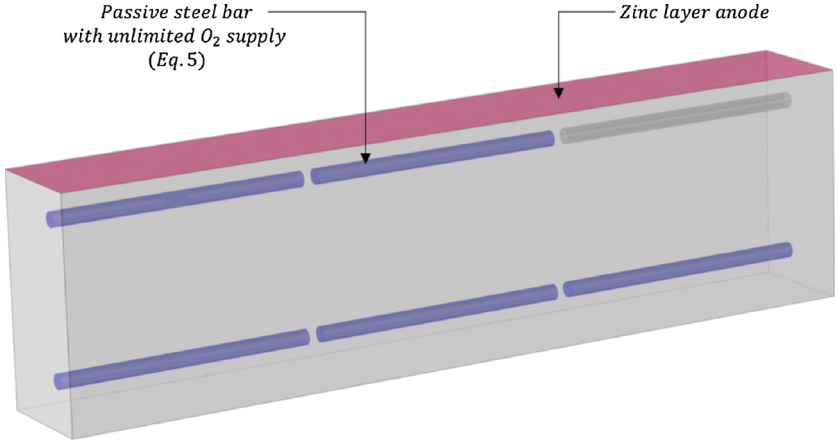

Fig. 8. Electrochemical model: geometry and boundary conditions.

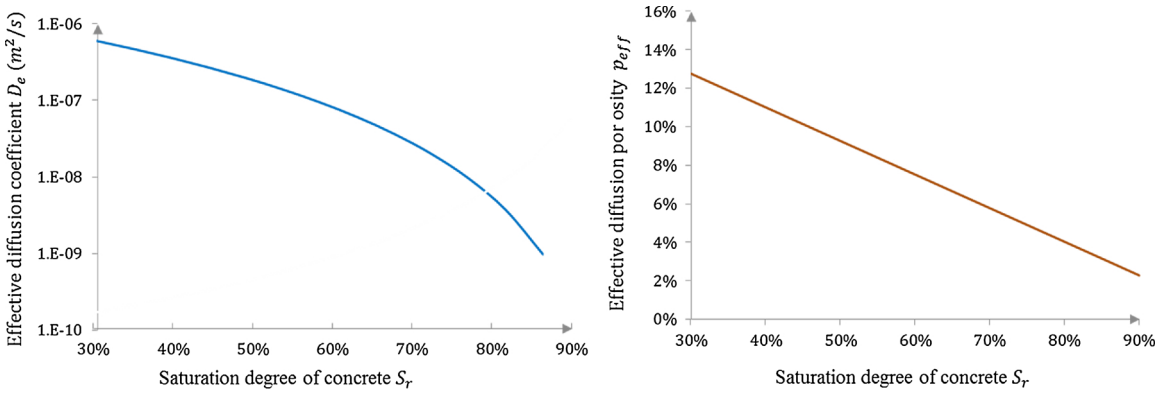

Fig. 9. Effective diffusion coefficient (left) and effective porosity (right) plotted versus saturation degree.

the atmospheric pressure (=101325 Pa).

A typical value of K_H for oxygen at 20 °C is about 3%.

According to Aachib et al. [15], the semi-empirical expression of effective diffusion coefficient of oxygen D_e ($m^2.\ s^{-1}$) is given by (Eq. (19)):

$$D_e = \frac{1}{p^2}(D_a^0.\ p_a^{3.3} + K_H.\ D_w^0.\ p_w^{3.3}) \tag{19}$$

where

- D_a^0 is the free oxygen diffusion coefficient in air (=1.8 10^{-5} $m^2.\ s^{-1}$),
- D_w^0 is the free oxygen diffusion coefficient in water (=2.5 10^{-9} $m^2.\ s^{-1}$),

The concrete is considered to be uniformly saturated by water, implying uniform scalar fields of effective diffusion coefficient and effective diffusion porosity. These simulation parameters are plotted versus saturation degree in Fig. 9 for a concrete porosity of 18%.

As briefly discussed above, the limiting current of oxygen reduction is the maximal value of cathodic current and may be calculated by assuming a total consumption of oxygen at the steel-concrete interface. Therefore, two types of Dirichlet boundary conditions are sufficient here to perform the simulation. They are given in Eq. (20) for the passive steel interfaces and Eq. (21) for outer, uncoated concrete surfaces exposed to air.

$$c = 0 \tag{20}$$

$$c = c_\infty = c_g\ p_{eff} \tag{21}$$

where c_∞ ($mol.\ m^{-3}$) is the oxygen concentration in concrete on outer surfaces.

Any other boundary of the geometric model is associated with an insulation condition as follows (Eq. 22):

$$J_n = 0 \tag{22}$$

where J_n is the normal flux of oxygen ($mol.\ m^{-2}.\ s^{-1}$).

Then, the limiting current of oxygen reduction I_{lim,O_2} results from the surface integration of the normal oxygen flux consumed at the whole passive steel surface S_p (Eq. (23)):

$$I_{lim,O_2} = \iint_{S_p} -4\,F\,J_n dS \tag{23}$$

The limiting current I_{lim,O_2} may be compared to the cathodic current estimated with the Electrochemical model I_p assuming an unlimited oxygen supply:

- $I_{lim,O_2} \gg I_p$: The rate of cathodic reaction is entirely controlled by charge transfer. The oxygen concentration field in the concrete volume is useless to assess the galvanic protection current here and the Electrochemical model is relevant.
- $I_{lim,O_2} \ll I_p$: The cathodic current density is entirely controlled by the rate of the mass transport and no longer depends on electrochemical processes. The potential field in the concrete volume is useless to obtain the galvanic protection current here and the Diffusion model is relevant.
- $I_{lim,O_2} \simeq I_p$: Both the charge transfer and the mass transport determine the overall reaction rate. The Multiphysics model is then necessary to perform reliable numerical simulations.

3.3. Multiphysics model

The Multiphysics model is built using the same constitutive equations, namely the local Ohm's law (Eq. (6)) and charge conservation (Eq. (7)) for electrical phenomena, Butler-Volmer behaviours for charge transfer phenomena, and Fick's first law adapted to porous media (Eq. (14)) and mass conservation for diffusion phenomena. The model coupling is performed by modifying the passive steel boundary conditions slightly.

Oxygen molecules reaching the cathodic surfaces (passive steel rods) are reduced to hydroxide ions OH^-. The time rate of OH^- ion production at passive steel surface S_p expresses the cathodic current density i_c, which can therefore be easily related to the normal oxygen flux consumed at the cathodic surface J_n ($mol.\ m^{-2}.\ s^{-1}$) as follows (Eq. (24)):

$$J_n = D_e \left.\frac{\partial c}{\partial n}\right|_{cathode} = \frac{i_c}{-4F} \tag{24}$$

The Butler-Volmer equation written as Eq. (5) and used as boundary condition in the electrochemical model involves an unlimited oxygen supply. As in the works by Kranc and Sagüés [17], a modified Butler-Volmer equation taking the mass transport of oxygen through concrete into account is used here to model steel cathodic behaviour as follows (Eq. (25)), the anodic behaviour being neglected here since steel is passive:

$$i = -i_{corr}\,\frac{c}{c_\infty}\exp\left(-\frac{\mathrm{Log}(10)(E - E_{corr})}{\beta_c}\right) \tag{25}$$

Therefore, the problem variables E and c are coupled thanks to the passive steel boundary condition. Thus, the solution of the coupled physical problem is obtained by determining:

- The concentration distribution of oxygen dissolved in the pore solution of the concrete,
- The electrical potential field and the protecting current distribution flowing in the concrete volume from the galvanic anode towards the reinforcing steel bars.

Fig. 10 illustrates the geometry and boundary conditions for the numerical simulation based on the Multiphysics model.

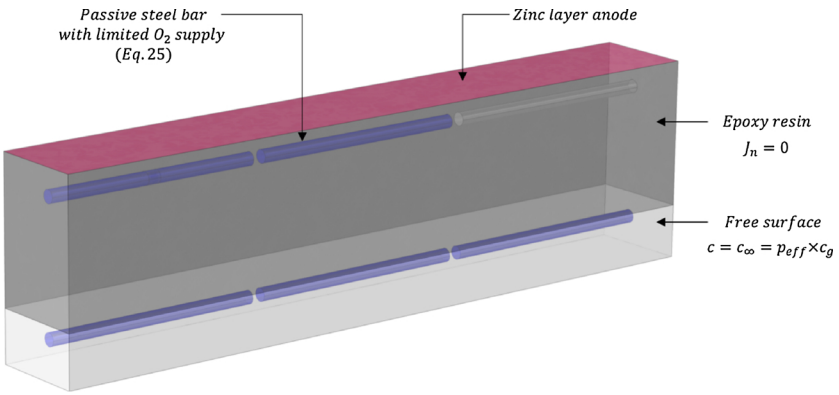

Fig. 10. Multiphysics model: geometry and boundary conditions.

4. Experimental validation of the numerical results

In this section, a preliminary numerical study is carried out in order to describe the effect of the water content of concrete on the behaviour of the cathodic protection system in the case of uniform moisture saturation in the concrete volume. Then, specific simulations of the two experiments presented in section 2 are presented and discussed. The simulated cathodic currents produced by individual steel bars (i.e. the galvanic protection current received by each steel bar) are compared with experimental results to highlight the robustness and reliability of the modelling approaches.

4.1. Preliminary numerical simulation of the effect of the concrete saturation degree

Here, a special attention is given to the effect of concrete water saturation on the cathodic protection current received by the steel bars in the case of uniform water distribution in the concrete volume. The numerical specimen reproduces the geometry and steel layout of the experimental beams presented in section 2. The three modelling approaches are involved here to cover the validity domains of the Electrochemical and Diffusion models. The Multiphysics model is then regarded as the only reliable numerical tool to correctly assess the galvanic protection current on the overall range of water saturation degrees.

Fig. 11 focuses on the specific current received by bar 1 (I_1), but the same qualitative results were observed for the other steel rods, giving different current magnitudes according to their respective locations in the concrete volume. The figure presents the numerical relationship between the water saturation degree and the bar current I_1. As stated above, this current represents the kinetics of the cathodic reaction at the surface of bar 1, which is actually the fraction of the ZLA galvanic protection current it receives. For water saturation degrees of less than 60%, it is observed that the Electrochemical model is asymptotically equivalent to the Multiphysics model. For such saturation degrees, the amount of oxygen at the concrete-steel interface is the same as at the free surfaces of the concrete structure. The kinetics of the ZLA galvanic system is therefore entirely controlled by charge transfer at the metal-concrete interfaces and by the electrical resistivity of the concrete.

Conversely, for water saturation degrees higher than 85%, asymptotic convergence of the Diffusion and Multiphysics models is observed, meaning that the Diffusion model provides good estimation of the level of galvanic protection for wet concrete conditions. Here, the oxygen reduction is faster than its transport from the external atmosphere

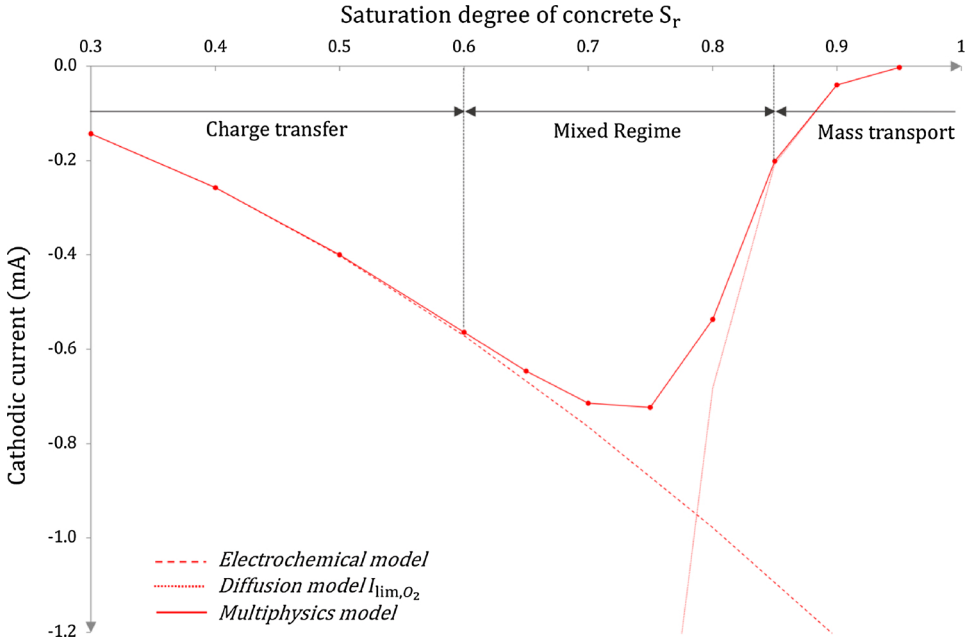

Fig. 11. Numerical simulations of the protection current received by the upper-layer bar 1 (I_1) as a function of the water saturation degree of concrete (based on the Electrochemical, Diffusion and Multiphysics models).

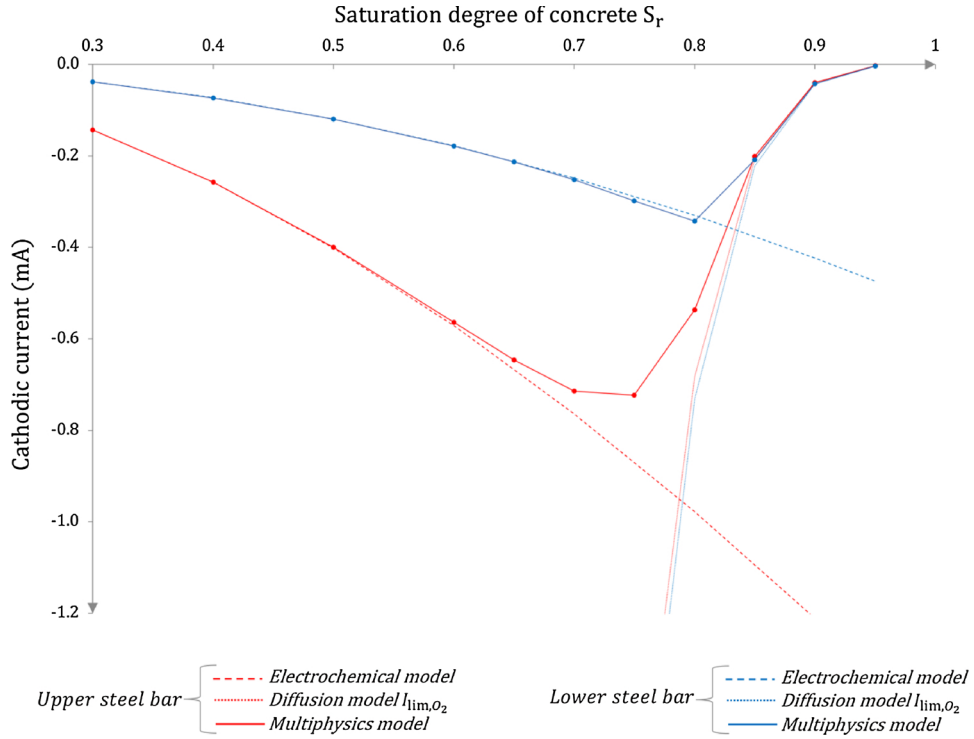

Fig. 12. Numerical simulations of the protection currents received by the upper-layer bar 1 (I_1 – red lines) and the lower-layer bar 4 (I_4 – blue lines) as a function of the water saturation degree of concrete (based on the Electrochemical, Diffusion and Multiphysics models) (For interpretation of the references to colour in this figure legend, the reader is referred to the web version of this article.).

towards the steel bars and the electrical resistivity is so low that it is not a control parameter. Therefore, the galvanic protection process is controlled by the kinetics of oxygen diffusion through the concrete. The limiting current of oxygen diffusion is reached and the total consumption of oxygen on passive steel areas is thus a reliable boundary condition.

In the 60% to 85% moisture saturation range (Mixed regime), both the charge transfer and the mass transport determine the overall reaction rate. The simplified assumptions involved in the Electrochemical and Diffusion models are then inaccurate, since both models lead to an overestimation of the protecting current. The existence of the Mixed regime results from the competition between oxygen diffusion and electrical resistivity for intermediate saturation degrees. This competition leads to the existence of an optimal water saturation degree for which the protecting current rate is maximal. Here, the optimal degree of water saturation is approximately 75% and the maximal protection current received by the bar 1 is found to be $-0.72\,mA$, corresponding to an average current density of $-135\,mA/m^2$ of steel.

Due to geometrical effects, in particular the respective locations of the passive steel bars with respect to the ZLA system, the Mixed regime and the optimal saturation degree may differ significantly among the reinforcements. Fig. 12 illustrates this statement by adding the relationship between saturation degree and protection current received by bar 4 (I_4), which is located under bar 1 in the concrete beam. It can be clearly seen that the current response relative to the Electrochemical model for bar 4 (blue dashed line) is significantly lower than that of bar 1 (red dashed line). This is simply explained by the by the fact that the I_4 current streamlines encounter higher electrolytic resistance (R_e) resulting from the greater electrical path length from the ZLA system at the top surface of the beam to the lower passive steel layer.

The global cathodic protection current streamlines are shown in Fig. 13 for a 60% - uniform saturation degree. The cross-section A-A reveals the ZLA current distribution towards bars 1 and 4 and the graphical streamline thickness and density around the bars represents the magnitude of the protection current they receive. The difference in electrical path length between ZLA to bar 1 and ZLA to bar 4 results in thicker and more dense current streamlines around bar 1, meaning a higher value for I_1 than for I_4. In Fig. 13, the cross section B-B shows that no protecting current reaches bar 3, since it was modelled as unconnected to the ZLA system, as in the experiments described in section 2.

However, at high saturation degrees, the Diffusion response of bar 4 is practically identical to that of bar 1 (Fig. 12). The similarity in these purely diffusive behaviours is explained by Fig. 14, which presents the oxygen flux streamlines responsible for the effective values of oxygen-reduction limiting currents at each passive steel rod. From the diffusive point of view, the location of the ZLA with respect to a specific steel bar has no influence, since the cathodic rate is only controlled by the amount of oxygen supplied. Therefore, here, the location of the steel bar with respect to the external surface of the concrete (where oxygen is available) is the most relevant influencing factor. In Fig. 13, it is observed that oxygen comes primarily from the lateral faces of the concrete beam. Therefore, the distance between the bars and the external faces is almost identical for either the upper or the lower steel bars, meaning that the oxygen-reduction limiting currents are very similar for all the steel bars.

From the lowered Electrochemical response of bar 4 (compared to bar 1) and its Diffusion response identical to that of bar 1, it is trivial to observe and understand that the Mixed regime region of bar 4 is shifted towards higher saturation degrees. For bar 4, the optimal saturation degree is about 80% and the associated maximum protection current is $-0.3\,mA$.

This preliminary numerical study highlights the difficulty of establishing global validity domains, in terms of range of saturation degree, for the Electrochemical and Diffusion models. Indeed, it has been demonstrated here that the validity domains depend on the steel bar under consideration and, in particular, its location with respect to the ZLA, but also with respect to the oxygen source. Therefore, except for very specific conditions (very dry concrete or very wet concrete), it appears hazardous to use the two simplified models for structures with

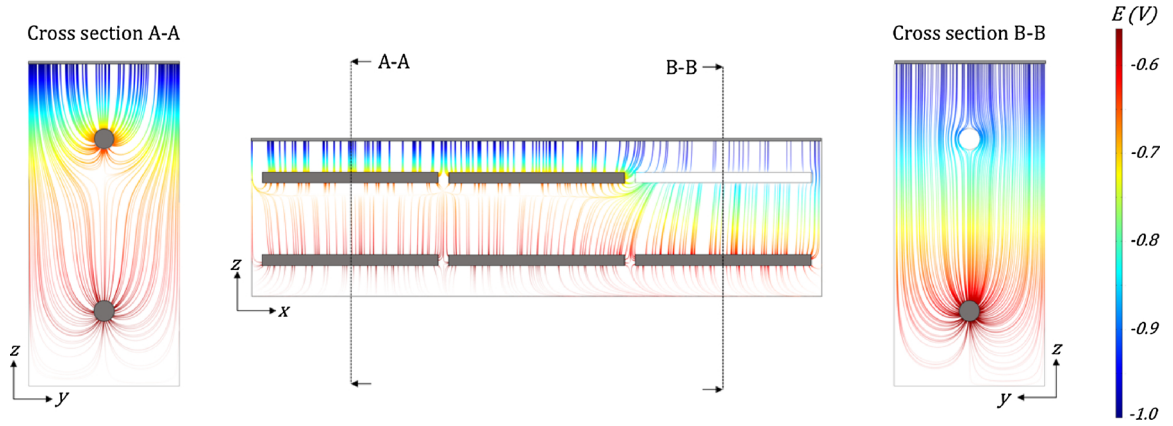

Fig. 13. Cathodic protection current streamlines and potential distribution within the concrete beam calculated with electrochemical model for a water saturation degree of concrete of 60%.

complex shapes, complex steel layouts or complex boundary conditions. The decision to use one of these models requires a careful assessment of whether or not it is applicable.

4.2. Numerical simulation of Test1 (unlimited oxygen supply) – Electrochemical model

This section addresses the numerical simulation of experimental Test 1. As briefly discussed in section 2, a complementary investigation revealed that a fairly uniform concrete saturation degree of 60% was achieved in the conditions of Test 1 after a natural-drying period in the air-conditioned test room. The saturation degree was measured on small concrete cylinders coming from the same concrete batch as the experimental specimen. At this level of hydric equilibrium, the oxygen diffusion mainly occurs in the gaseous phase of the cementitious matrix, so there is no significant limitation on oxygen transport in the concrete. Taking into account the conclusions of the preliminary numerical study above, the numerical simulation of Test 1 using the Electrochemical model is relevant since the oxygen supply is considered as sufficient to fuel cathodic reactions on each steel-concrete interface.

Fig. 15 presents a direct comparison of numerical and experimental protecting currents for each passive steel bar. It can be observed that the Electrochemical model provides a rather good estimation of the protecting current distribution over the steel rods for a uniform water saturation degree of 60%, which corresponds well to the hydric equilibrium state of the concrete beams during the current monitoring. The simulated global macrocell current flowing from the zinc layer anode to the reinforcing bars ($-1.8\,mA$) is in accordance with the total output current measured experimentally ($-1.79\,mA$).

It is observed that the effect of the disconnection of bar 3, discussed in section 2, is also visible on the numerical simulation, as expected. Despite a numerical value of I_1 higher than the experimental one, I_2 remains higher compared to I_1, as does as I_6 compared to I_4 and I_5.

The current and potential distributions within the concrete beam corresponding to Test 1 (60% saturation degree) are displayed in Fig. 13 using a rainbow colour range to express local potential values. As expressed above, the line thickness reflects the norm of the local current density vector i. Thin lines correspond to a low ionic current while thick lines reflect a higher current density. Qualitatively, the masking effect of the upper steel layer is illustrated by the gradual decrease of the line thickness over depth due to an increasing ohmic resistance. By comparing cross-sections A-A and B-B, it can be clearly seen that bar 6 (B-B) receives more protecting current from the ZLA than bar 4 does, since the unconnected bar 3 does not produce any masking effect.

4.3. Numerical simulation of Test 2 (limited oxygen supply) – Multiphysics model

Unlike in Test 1, the moisture content of the coated concrete beam (Test 2) cannot be assessed experimentally. The uncoated lower part of the specimen (below the lower steel layer) had been stored out of water, leading to a partially saturated concrete. Conversely, the coated upper part of the beam was close to the total water saturation since it was sealed before drying.

The hydric field within the concrete volume therefore has to be

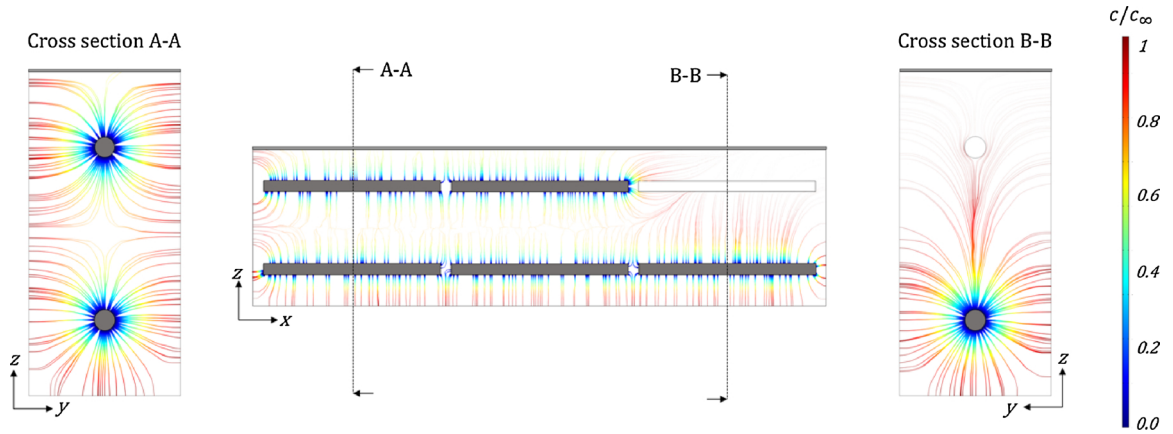

Fig. 14. Oxygen flux streamlines and oxygen supply distribution within the concrete slab calculated with the diffusive model for a water saturation degree of concrete of 60%.

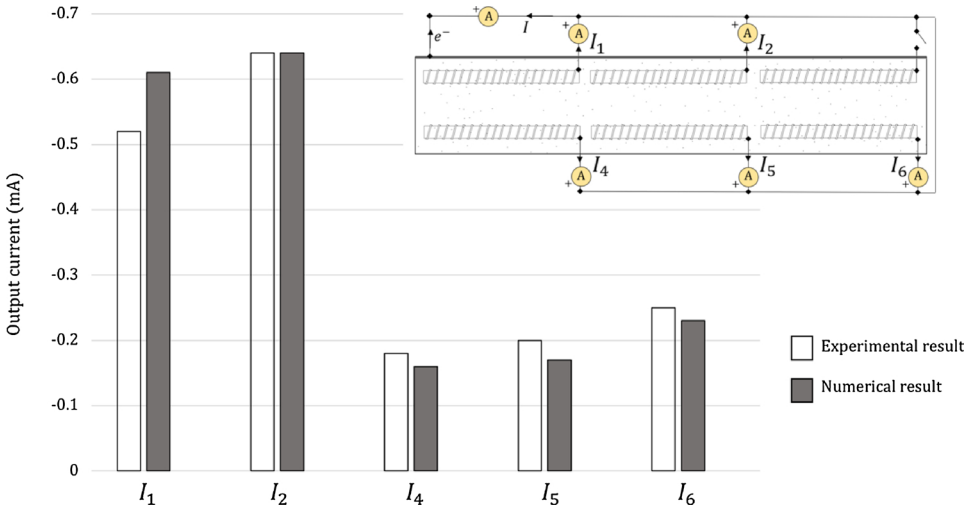

Fig. 15. Comparison of experimental and simulated protecting current distributions – Test 1 (unlimited oxygen supply).

inferred by appropriate assumptions. Nevertheless, the mass transport cannot be neglected when simulating the measured output currents from the connected bars, since the oxygen supply is limited, at least in the upper coated part of the specimen, and only the Multiphysics model is relevant here.

To infer the hydric field in the concrete volume in the conditions of Test 2, preliminary numerical simulations based on the Multiphysics model were carried out (Fig. 16). As a first approximation, the numerical model may be considered as two distinct domains with different saturation degrees. It should be noted here that the modelling of water transport through concrete is outside the scope of this study. The concrete in the upper, coated, part of the specimen is assumed to have a uniform degree of saturation, labelled S_{r1}, and the concrete in the lower, uncoated, part is associated with a different saturation degree, labelled S_{r2}. The saturation degree of the coated part S_{r1} was inferred to be 90%, which is a realistic value for saturated concretes and an accurate assumption. Then, a series of numerical simulations were performed by varying the saturation degree, S_{r2}, of the lower part, which is more difficult to assess reliably. The variation range of S_{r2} involved in the simulations was between 60 and 80%. The simulation results are displayed in Fig. 16 as the numerical relationship between the protection currents received by bars 1 and 4 and the saturation degree of the lower, uncoated, concrete volume, S_{r2}.

As observed in the experiment of Test 2, the numerical simulations show a significantly higher cathodic current for bar 4 than for bar 1. More generally, a higher fraction of the galvanic protection current appears to be collected by the lower steel bars due to the very low amount of oxygen in the upper part of the concrete. The robustness of the Multiphysics modelling approach is highlighted here since it is able to reproduce experimental data. For saturation degrees S_{r2} lying between 60 and 75%, the current received by bar 4 is stabilized at around $-0.8\,mA$, meaning that charge transfer controls the cathodic reaction in such a saturation range of the lower concrete part. At higher saturation degrees ($S_{r2} = 80\,\%$), the protection current is lowered by about 20%, meaning that oxygen access in the lower concrete part is more difficult. Regarding the behaviour of bar 1, the very low cathodic current is linearly lowered with the increase in S_{r2}. This relationships results from the fact that, even for the upper steel bar, the very low amount of oxygen available for cathodic reaction comes from the lower part of the beam in such a testing condition.

Regarding the relative stability of the protection current in the S_{r2} saturation range from 60 to 75%, the mid-range value of 67.5% was chosen to infer the saturation degree of the lower concrete volume in the conditions of Test 2. Due to this stability, the possible error with

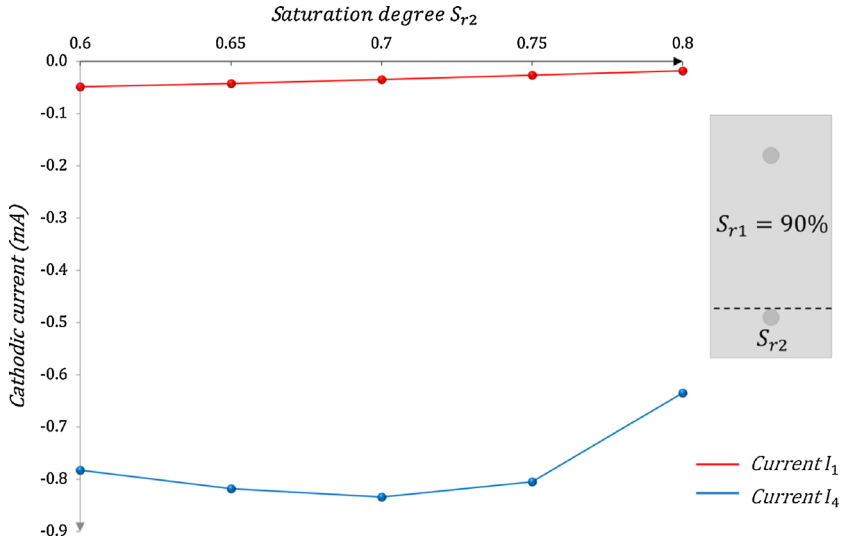

Fig. 16. Simulated output currents I_1 (in red) and I_4 (in blue) as a function of the saturation degree Sr_2 within coated concrete beam (For interpretation of the references to colour in this figure legend, the reader is referred to the web version of this article.).

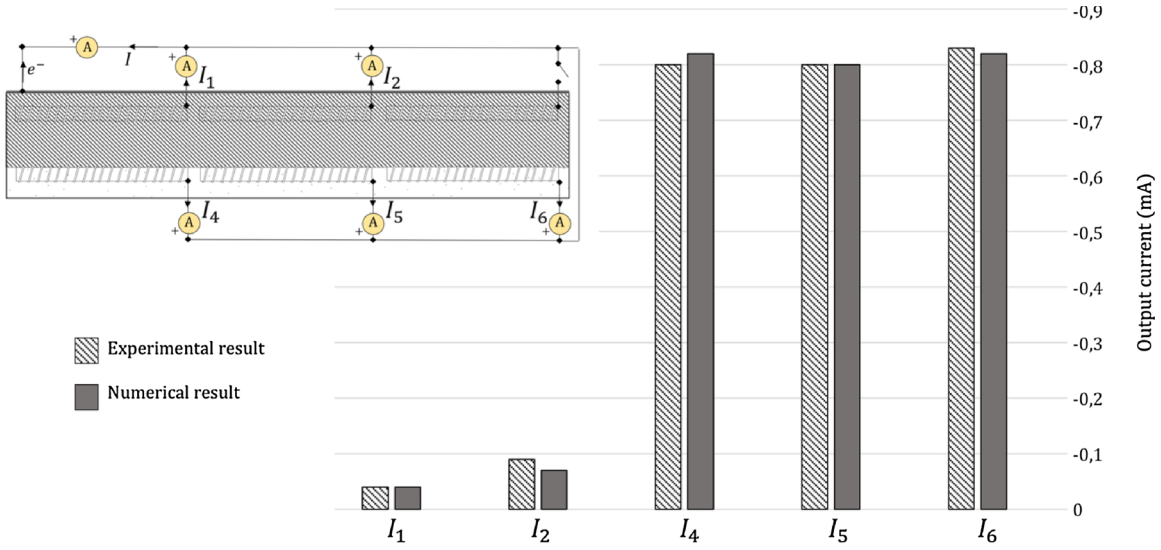

Fig. 17. Comparison of experimental and simulated protecting current distributions – Test 2 (limited oxygen supply at the upper steel layer).

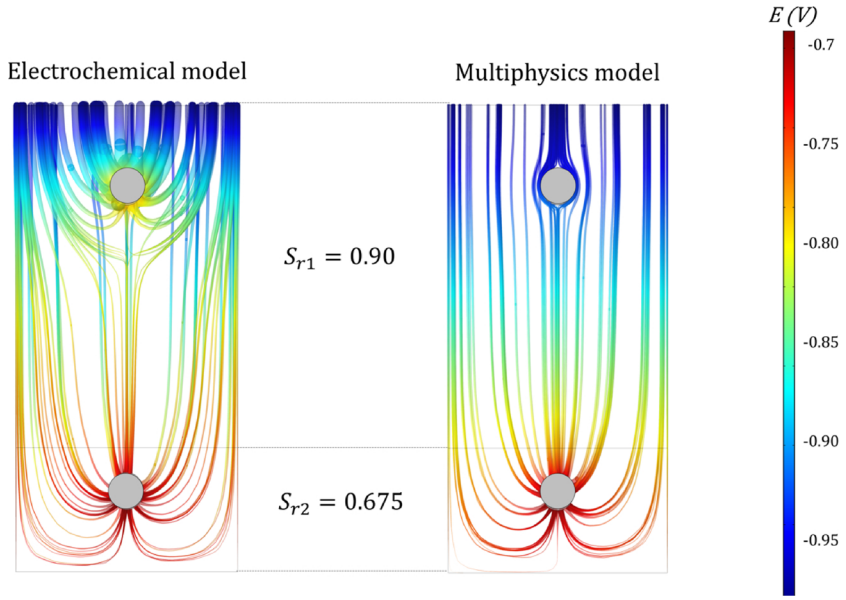

Fig. 18. Comparison of the numerical protection current streamlines and local potential fields within the coated concrete beam (cross section A-A) based on Electrochemical (left) and Multiphysics (right) models for a hydric field of 90% in the upper part of the specimen and 67.5% in the lower part.

respect to the effective saturation range produced only very slight deviations in the simulated currents.

Fig. 17 presents a direct comparison of numerical and experimental protecting currents for each passive steel bar in the conditions of Test 2. The experimental current distribution appears almost identical to the numerical one, estimated with the Multiphysics model for the following hydric field: $S_{r1} = 90\,\%$ and $S_{r2} = 67.5\,\%$. The global macrocell current flowing from the zinc layer anode to the steel network is, moreover, found to be equal to the galvanic current measured experimentally ($-\,2.55\,mA$).

The Multiphysics model appears relevant and robust here to describe physical phenomena occurring in the conditions of Test 2. Neglecting the effect of oxygen transport, by implementing a pure Electrochemical model, would lead to considerable error in such a case. In order to confirm this statement, Fig. 18 compares current distributions from the ZLA to the steel bars, achieved by the Electrochemical model (left) and by the Multiphysics model (right) in the conditions of Test 2.

By considering charge transfer and concrete electrical resistivity as the only limiting factors in the Electrochemical simulation (left), the protection current is distributed in a very different way from that achieved with the multiphysics interaction between the electrochemical process and oxygen diffusion (right). In such environmental conditions, the Electrochemical model leads to a significantly higher fraction of the protection current collected by the upper steel layer, which was experimentally demonstrated to be irrelevant. The Electrochemical model is clearly not suitable here, since the mass transport, as well as the charge transfer and the concrete resistivity, determine the overall reaction rate.

5. Conclusion

This paper addresses the spatial distribution of the galvanic protection current provided by a Zinc Layer Anode system (ZLA) over a reinforcing steel network embedded in a concrete beam. Two specific cases are studied: unlimited and limited oxygen supply to the steel bars. The results of original experiments carried out to assess the current distribution in the concrete specimen are discussed for both oxygen-

supply conditions. The theoretical details of three possible modelling approaches are then presented. Finally, numerical simulations of the experiments are reported and discussed. The findings of this research work provide original insight into the physical complexity relative to the galvanic protection of reinforcing steel in concrete and show that the classical design approach of such protecting systems should be reconsidered.

Despite a few research works in the literature on the interaction between electrochemical processes and oxygen diffusion, the electrical resistivity is still considered as the predominant control parameter of a galvanic protection system. This statement is implicitly the reason why only the steel bars close to the anodic system are usually considered by designers as being concerned in the galvanic exchange. In this paper, it is demonstrated that the oxygen transport can be neglected only in the case of a dry concrete. Moreover, in some specific, but realistic and possibly quite frequent, conditions, distant steel bars may collect more protecting current than steel bars close to the anodic system.

Actually, the global system equilibrium, i.e. the natural macrocell current supplied by the ZLA and its spread over the whole steel network in the concrete volume, results from some predominant influencing factors:

- The geometry of the reinforced concrete element, including the steel layout;
- The field of electrical conductivity of the concrete;
- The charge transfer processes at the metal-concrete interfaces;
- The oxygen supply to the steel bar.

By considering the last three influencing factors mentioned above, it is trivial to deduce that the volumetric water content of the concrete is a key issue since an increase in the water saturation degree leads simultaneously to:

- An increase in the electrical conductivity and therefore in the charge transfer kinetics, which tend to increase the global galvanic protection current exchanged between the ZLA system and the steel network;
- A decrease in the oxygen supply to the cathodic areas, which tends to decrease the galvanic protection current.

Consequently, for varying water saturation degrees of the concrete, the galvanic protection system equilibrium is determined by the competition between the charge transfer processes and the oxygen transport through the concrete. Due to these opposite effects of moisture content on oxygen diffusivity and charge transfer (related to electrical conductivity of the concrete), an optimal water saturation degree exists, for which the macrocell current produced by the zinc layer anode is maximal. Moreover, taking account of the possible non-uniformity in the concrete water saturation, the steel layer immediately next to the sacrificial anode does not systematically collect the highest fraction of the protecting current. One of the experiments presented in the paper clearly demonstrates that distant steel bars may collect much more protection current than the ones close to the ZLA, providing some specific conditions hold for oxygen distribution in the concrete volume.

Nevertheless, such conditions can occur in real structures, especially in the case of ZLA galvanic protection, for which the oxygen supply towards the shallow steel bars may be limited, or even avoided by the ZLA sheet itself. The galvanic protection current is then spread over more distant steel bars where the oxygen amount is sufficient to fuel the cathodic reaction. So, when designing such galvanic protecting systems, considering only the closest steel bars (with respect to the anodic system) is likely to lead to erroneous predictions of the cathodic protection efficiency.

Regarding the physical complexity related to the effective distribution of the protection current on the whole steel network, it appears that the design of cathodic protection systems by using unjustified assumptions and simple analytical rules may lead to inconsistent solutions. Due to the real 3D nature of the problem, only appropriate numerical simulations based on robust models can provide some physical justifications to the design of a specific cathodic protection system adapted to a specific reinforced concrete element, with its own environmental conditions, its own geometry… The qualitative and quantitative agreement between experimental and numerical results presented in this paper shows that robust and parsimonious modelling approaches are available to improve the cathodic protection design.

Further scientific developments are currently underway to improve these modelling approaches by taking account of the water transport within the pore network, in order to implement non-uniform fields of water saturation rather than uniform fields applied over the whole concrete volume. Moreover, the seasonal variations in the structure environmental conditions imply that the galvanic equilibrium should be addressed as a time dependent problem, with a time-varying protection current value and distribution.

References

[1] R. Francois, Effect of damage in reinforced concrete on carbonation or chloride penetration, Cem. Concr. Res. (9) (1988).
[2] NACE International, CP-2 Cathodic Protection Technician Course Manual, Nace, Houston 49 (2) (2000) 80–102 2000.
[3] ISO 12696:2016 Cathodic Protection of Steel in Concrete, (2016) no. 122457.
[4] S. Laurens, P. Hénocq, N. Rouleau, F. Deby, E. Samson, J. Marchand, B. Bissonnette, Steady-state polarization response of chloride-induced macrocell corrosion systems in steel reinforced concrete - Numerical and experimental investigations, Cem. Concr. Res. 79 (2016) 272–290.
[5] A. Clément, S. Laurens, G. Arliguie, D. Deby, Numerical study of the linear polarization resistance technique applied to reinforced concrete for corrosion assessment, Eur. J. Environ. Civ. Eng. (2012).
[6] D. Garcia, S. Laurens, S. Panin, Electrochemical behavior of zinc layer anodes used for galvanic protection of steel in reinforced concrete, RILEM Tech. Lett. 3 (2018) 59–65.
[7] M. Raupach, Investigations on the influence of oxygen on corrosion of steel in concrete—part 2, Mater. Struct. 29 (4) (1996) 226–232.
[8] B. Huet, V. L'hostis, G. Santarini, D. Feron, H. Idrissi, Steel corrosion in concrete: determinist modeling of cathodic reaction as a function of water saturation degree, Corros. Sci. 49 (4) (2007) 1918–1932.
[9] L. Bertolini, E. Redaelli, Throwing power of cathodic prevention applied by means of sacrificial anodes to partially submerged marine reinforced concrete piles: results of numerical simulations, Corros. Sci. 51 (9) (2009) 2218–2230.
[10] M.M.S. Cheung, C. Cao, Application of cathodic protection for controlling macrocell corrosion in chloride contaminated RC structures, Constr. Build. Mater. 45 (2013) 199–207.
[11] J. Ožbolt, G. Balabanić, M. Kušter, 3D Numerical modelling of steel corrosion in concrete structures, Corros. Sci. 53 (12) (2011) 4166–4177.
[12] J. Warkus, M. Raupach, J. Gutikers, Numerical modelling of corrosion - Theoretical backgrounds, Mater. Corros. 57 (8) (2006) 614–617.
[13] J. Gulikers, M. Raupach, Numerical models for the propagation period of reinforcement corrosion: Comparison of a case study calculated by different researchers, Mater. Corros. 57 (8) (2006) 618–627.
[14] Stratégie d'évaluation Non destructive pour la Surveillance des Ouvrages en béton – SENSO" Rapport Final, 2009, 274p.
[15] M. Aachib, M. Mbonimpa, M. Aubertin, Measurement and predictions of the oxygen diffusion coefficient in unsaturated media, with applications to soil covers, Water Air Soil Pollut. 156 (2004) 163–193.
[16] R. Millington, R. Shearer, Diffusion in aggregated porous media, Soil Sci. (1971).
[17] S.C. Kranc, A.A. Sagüés, Detailed modeling of corrosion macrocells on steel reinforcing in concrete, Corros. Sci. 43 (7) (2001) 1355–1372.